Nonlinear Dynamics **29:** 235–250, 2002.

Describing Function Analysis of Systems with Impacts and Backlash

R. S. BARBOSA and J. A. TENREIRO MACHADO
Department of Electrotechnical Engineering, Institute of Engineering of Porto, Rua Dr. António Bernardino de Almeida, P-4200-072 Porto, Portugal

(Received: 28 February 2002; accepted: 12 March 2002)

Abstract. This paper analyzes the dynamical properties of systems with backlash and impact phenomena based on the describing function method. It is shown that this type of nonlinearity can be analyzed in the perspective of the fractional calculus theory. The fractional-order dynamics is illustrated using the Nyquist plot and the results are compared with those of standard models.

Keywords: Describing function, backlash, fractional-order systems, modeling.

1. Introduction

Fractional Calculus (FC) is a branch of mathematics that deals with the generalization of the operation of differentiation and integration to an arbitrary order. The theory of FC is a well-adapted tool to the modeling of many physical phenomena, allowing the description to take into account some peculiarities that classical integer-order models simply neglect. For this reason, the first studies and applications involving FC were developed in the domain of fundamental sciences, namely in physics [5] and chemistry [24]. Besides the intensive research carried out in the area of pure and applied mathematics [1–7], FC has found applications in fields such as viscoelasticity/damping [8–13], chaos [14], fractals [15–17], biology [18], electronics [19], signal processing [20], diffusion and wave propagation [21–23], modeling and identification [25, 26], electromagnetism [27, 28] and automatic control [29–33]. Nevertheless, in spite of the work that has been done in the area, many aspects remain to be investigated.

The phenomenon of vibration with impacts occurs in many branches of technology, namely in impact machines, vibration dampers and shakers, where it plays a very useful role. On the other hand, its occurrence is often undesirable, because it causes additional dynamic loads, as well as faulty operation of machines and devices. Despite many investigations that have been carried out so far, this phenomenon is not fully understood yet, mainly due to the considerable randomness and diversity of reasons underlying the energy dissipation involving the dynamic effects [36–38].

In this paper, we investigate the dynamics of systems that contain backlash and impacts. It is shown that these nonlinear phenomena can exhibit a fractional-order dynamics revealing that the FC is an adequate tool for the analysis of these systems.

In this perspective, this paper investigates the dynamics of systems with backlash and impact phenomena through the describing function method.

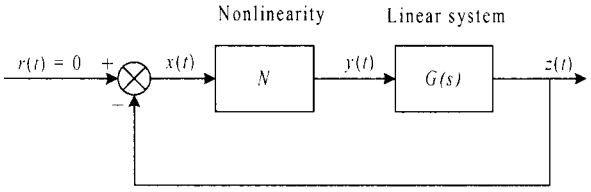

Figure 1. Basic nonlinear feedback system for describing function analysis.

Bearing these ideas in mind, the present paper is organized as follows. Section 2 introduces the fundamental aspects of the theory of the describing function method. Section 3 studies the describing function of systems with and without impacts. The results are compared with classical models of systems with simple geometric backlash. Finally, Section 4 draws the main conclusions and addresses perspectives towards future research.

2. Describing Function Analysis

The Describing Function (DF) is one of the possible methods that can be adopted for the analysis of nonlinear systems [35]. The basic idea is to apply a sinusoidal signal to the input of the nonlinear element and to consider only the fundamental component of the signal appearing at the output of the nonlinear system. Then, the ratio of the corresponding phasors (output/input) of the two sinusoidal signals represents the DF of the nonlinear element. The use of this concept allows the adaptation of the Nyquist stability test to a nonlinear system detection of a limit cycle, namely the prediction of its approximate amplitude and frequency.

In this line of thought, we consider the control-loop with one nonlinear element depicted in Figure 1.

We start by applying a sinusoid to the nonlinearity input:

$$x(t) = X\cos(\omega t). \tag{1}$$

At steady-state the output of the nonlinear characteristic, $y(t)$, is periodic and, in general, it is nonsinusoidal. If we assume that the nonlinearity is symmetric with respect to the variation around zero, the Fourier series becomes

$$y(t) = \sum_{k=1}^{\infty} Y_k \cos(k\omega t + \phi_k), \tag{2}$$

where Y_k and ϕ_k are the amplitude and the phase shift of the kth harmonic component of the output $y(t)$, respectively.

In the DF analysis, we assume that only the fundamental harmonic component of $y(t)$, Y_1, is significant. Such assumption is often valid since the higher-harmonics in $y(t)$, Y_k for $k = 2, 3, \ldots$, are usually of smaller amplitude than the amplitude of the fundamental component, Y_1. Moreover, most systems are 'low-pass filters' with the result that the higher-harmonics are further attenuated.

Thus the DF of a nonlinear element, $N(X, \omega)$, is defined as the complex ratio of the fundamental harmonic component of output $y(t)$ with the input $x(t)$:

$$N(X, \omega) = \frac{Y_1}{X} e^{j\phi_1}, \tag{3}$$

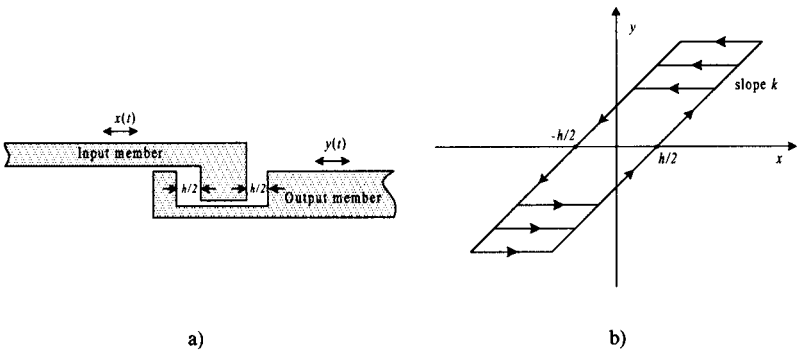

Figure 2. Static backlash nonlinearity: (a) geometric model, (b) input-output characteristic.

where X is the amplitude of the input sinusoid $x(t)$ and Y_1 and ϕ_1 are the amplitude and the phase shift of the fundamental harmonic component of the output $y(t)$, respectively.

In general, $N(X, \omega)$ is a function of both the amplitude X and the frequency ω of the input sinusoid. For nonlinear systems that do not involve energy storage, the DF is merely amplitude-dependent, that is $N = N(X)$. If it is not the case, we may have to adopt a numerical approach because, usually, it is impossible to find a closed-form solution.

For the nonlinear control system of Figure 1, we have a limit cycle if the sinusoid at the nonlinearity input regenerates itself in the loop, that is:

$$G(j\omega) = -\frac{1}{N(X, \omega)}. \tag{4}$$

Note that (4) can be viewed as the characteristic equation of the nonlinear feedback system of Figure 1. If (4) can be satisfied for some value of X and ω, a limit cycle is *predicted* for the nonlinear system. Moreover, since (4) applies only if the nonlinear system is in a steady-state limit cycle, the DF analysis predicts only the presence or the absence of a limit cycle and cannot be applied to analysis for other types of time responses.

3. Analysis of Systems with Backlash and Impact Phenomena

In this section, we use the DF method to analyze systems with backlash and impact phenomena. We start by considering the standard static model and afterwards we study the case of dynamic backlash (i.e. with the impact phenomena). Finally, we compare the results of the two types of approximations.

3.1. Static Backlash

Here, we consider the phenomena of clearance without the effect of the impacts, which is usually called *static backlash*. The model and its input-output characteristic are shown in Figure 2.

By applying a sinusoidal signal $x(t) = X \sin(\omega t)$ at the input member, the DF of the static backlash is given by the following expression [34]:

$$N(X, \omega) = \begin{cases} 0, & X \leq h/2, \\ \dfrac{k}{2}\left[1 - N_s\left(\dfrac{X/h}{1 - X/h}\right)\right] - j\dfrac{2kh(X - h/2)}{\pi X^2}, & X > h/2, \end{cases} \tag{5}$$

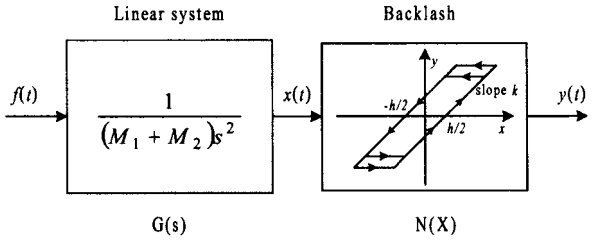

Figure 3. Classical backlash model.

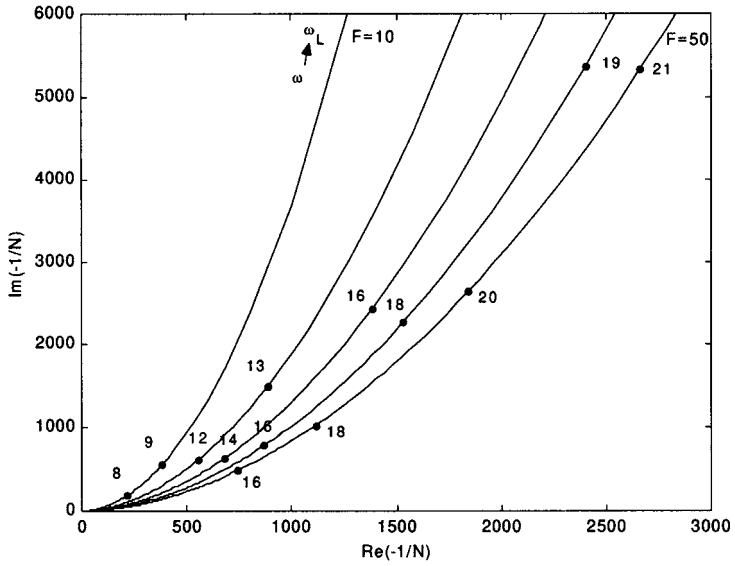

Figure 4. Nyquist plot of $-1/N(F, \omega)$ for the system of Figure 3, $F = \{10, 20, 30, 40, 50\}$ N, $0 < \omega < \omega_L$, $M_1 = M_2 = 1$ kg and $h = 10^{-1}$ m.

$$N_s(z) = \frac{2}{\pi}\left[\sin^{-1}\frac{1}{z} + \frac{1}{z}\cos\left(\sin^{-1}\frac{1}{z}\right)\right]. \tag{6}$$

The classical backlash model corresponds to the DF of a linear system of a single mass $M_1 + M_2$ followed by the geometric backlash having as input and as output the position variables $x(t)$ and $y(t)$, respectively, as depicted in Figure 3.

For a sinusoidal input force $f(t) = F\cos(\omega t)$ the condition $X = h/2$ leads to the limit frequency ω_L applicable to this system:

$$\omega_L = \left[\frac{2}{h}\frac{F}{(M_1 + M_2)}\right]^{1/2}. \tag{7}$$

Figure 4 shows the Nyquist plot of $-1/N(F, \omega) = -1/[G(j\omega)N(X)]$ for the system of Figure 3 for several values of the input force F.

This approach to the backlash study is based on the adoption of a geometric model that neglects the dynamic phenomena involved during the impact process. Due to this reason often real results differ significantly from those predicted by that model.

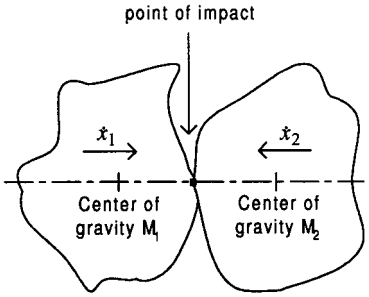

Figure 5. Representation of a central impact, with initial velocities $\dot{x}_1$ and $\dot{x}_2$.

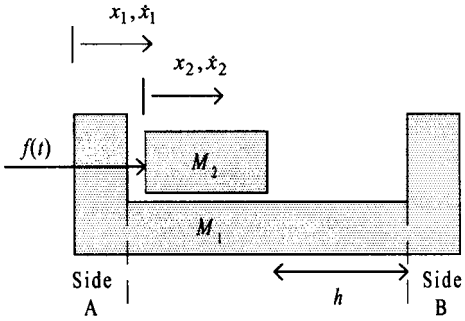

Figure 6. System with two masses subjected to dynamic backlash.

3.2. Dynamic Backlash

In this section, we consider the impact phenomenon based on the laws of conservation of momentum and an empirical manifestation of the conservation of energy. This approach provides information on the net change in velocity of each body involved in the impact, the net impulse, and the energy-exchange processes accompanying the impact. We consider the case of two bodies colliding on surfaces which are normal to the common line connecting their centers of mass and that have velocity components only along this common line. With these restrictions no rotational or sliding effects occur. This specific case is called a *central impact* and is illustrated in the conceptual model of Figure 5.

The proposed mechanical model consists on two masses (M_1 and M_2) subjected to backlash and impact phenomenon as shown in Figure 6.

It is straightforward to see that a collision between the masses M_1 and M_2 occurs when $x_1 = x_2$ or $x_2 = h + x_1$. In this case, we can compute the velocities of masses M_1 and M_2 after the impact ($\dot{x}_1'$ and $\dot{x}_2'$) by relating them to the previous values ($\dot{x}_1$ and $\dot{x}_2$) through Newton's law:

$$(\dot{x}1_1 - \dot{x}1_2) = -\varepsilon(\dot{x}_1 - \dot{x}_2), \quad 0 \leq \varepsilon \leq 1, \tag{8}$$

where ε is the coefficient of restitution that represents the dynamic phenomenon occurring in the masses during an impact. In the case of a fully plastic (*inelastic*) collision $\varepsilon = 0$, while in the *ideal elastic* case $\varepsilon = 1$.

The principle of conservation of momentum requires that the momentum, immediately before and immediately after the impact, must be equal:

$$M_1\dot{x}_1' + M_2\dot{x}_2' = M_1\dot{x}_1 + M_2\dot{x}_2. \tag{9}$$

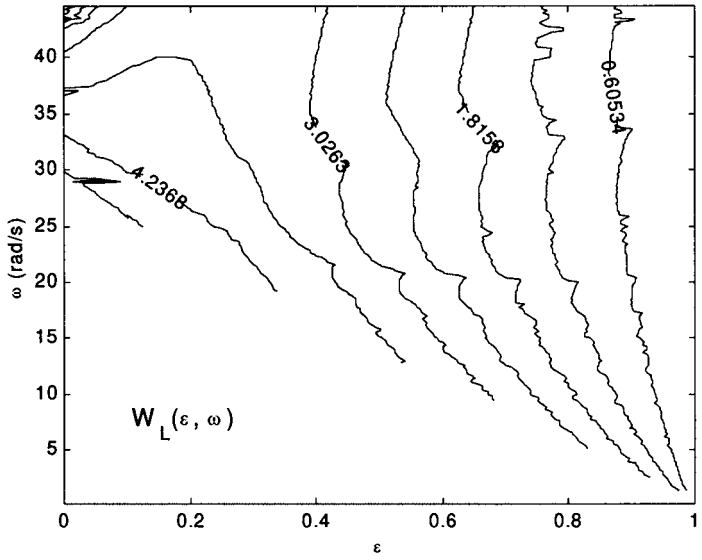

Figure 7. Contour plot of energy loss W_L vs. the exciting frequency ω and the coefficient of restitution ε, for an input force $F = 50$ N, $M_1 = M_2 = 1$ kg and $h = 10^{-1}$ m.

From (8–9), we can find the sought velocities of both masses after an impact:

$$\dot{x}_1' = \frac{\dot{x}_1(M_1 - \varepsilon M_2) + \dot{x}_2(1+\varepsilon)M_2}{M_1 + M_2}, \tag{10}$$

$$\dot{x}_2' = \frac{\dot{x}_1(1+\varepsilon)M_1 + \dot{x}_2(M_2 - \varepsilon M_1)}{M_1 + M_2}. \tag{11}$$

The total kinetic energy loss E_L at an impact is determined by

$$E_L = \frac{1-\varepsilon^2}{2}\frac{M_1 M_2}{M_1 + M_2}(\dot{x}_1 - \dot{x}_2)^2. \tag{12}$$

The validity of the proposed model is restricted to frequencies of the exciting input force $f(t)$ higher than a cut-off frequency ω_C. This frequency was determined numerically by considerations on the energy processes occurring during the impact process arriving to the approximate expression:

$$\omega_C \approx \left[\left(2\frac{F}{M_2 \cdot h}\right)^2 (1-\varepsilon)^5\right]^{1/4}. \tag{13}$$

Figures 7 and 8 illustrate the energy and power losses (i.e. W_L and P_L) vs. the exciting frequency ω and the coefficient of restitution ε. As expected, the energy (and the power) loss decreases as the coefficient of restitution increases. Moreover, as $\varepsilon \to 1$ it yields $\omega_C \to 0$, which is in accordance with Equation (13).

On the other hand, there is also a limiting frequency ω_L determined by application of Newton's law to mass M_2, that is $f(t) = M_2\ddot{x}_2(t)$. Considering an input signal $f(t) = F\cos(\omega t)$

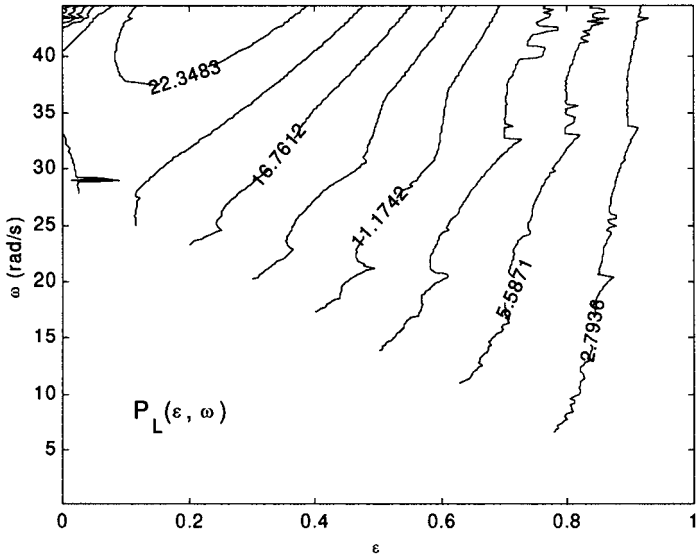

Figure 8. Contour plot of power loss P_L vs. the exciting frequency ω and the coefficient of restitution ε, for an input force $F = 50$ N, $M_1 = M_2 = 1$ kg and $h = 10^{-1}$ m.

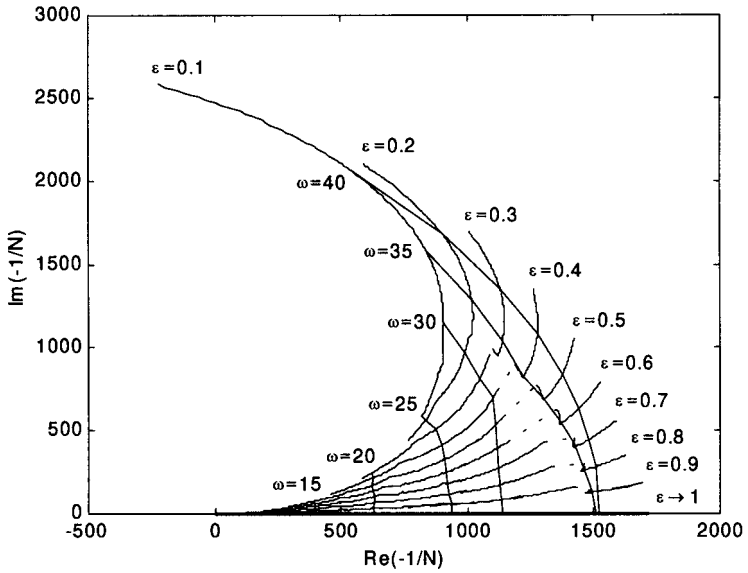

Figure 9. Nyquist plot of $-1/N(F, \omega)$ for the dynamic backlash, $F = 50$ N and $\varepsilon = \{0.1, \ldots, 0.9\}$.

and solving for $x_2(t)$ we arrive at an expression for ω_L when the amplitude of the displacement is within the clearance $h/2$, yielding

$$\omega_L = 2\left(\frac{F}{h \cdot M_2}\right)^{1/2}. \tag{14}$$

For the system model of Figure 6 we can calculate numerically the Nyquist diagram of $-1/N(F, \omega)$ for a sinusoidal input force $f(t) = F\cos(\omega t)$ applied to mass M_2 while considering as output position $x_1(t)$ of mass M_1.

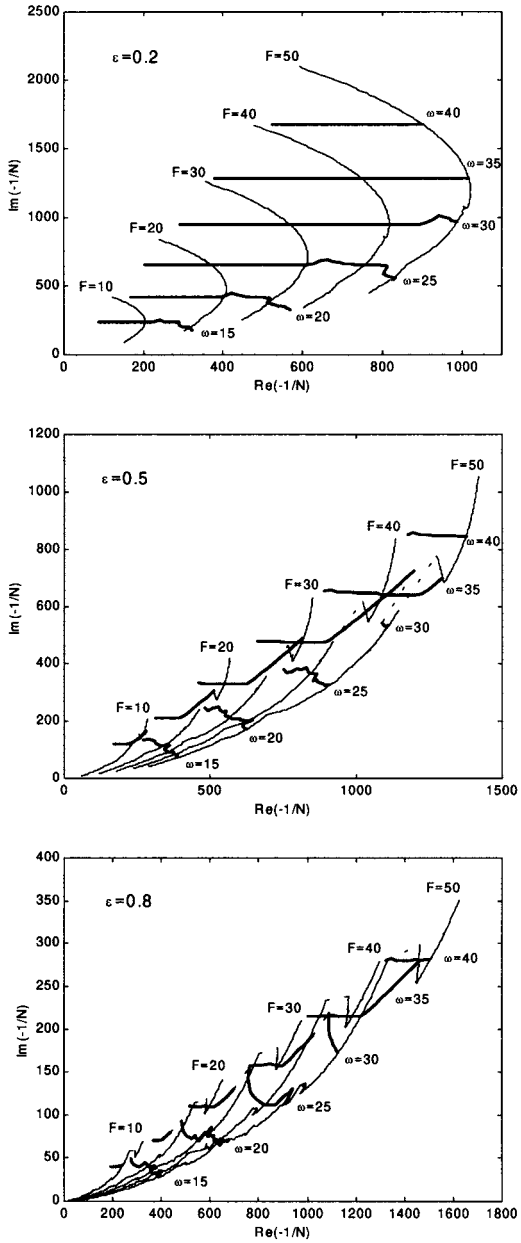

Figure 10. Nyquist plot of $-1/N(F, \omega)$ for a system with dynamic backlash, $F = \{10, 20, 30, 40, 50\}$ N and $\varepsilon = \{0.2, 0.5, 0.8\}$.

The values of the parameters adopted in the subsequent simulations are $M_1 = M_2 = 1$ kg and $h = 10^{-1}$ m. Figures 9 and 10 show the Nyquist plots for an input force $F = 50$ N and $\varepsilon = \{0.1, \ldots, 0.9\}$ and for $F = \{10, 20, 30, 40, 50\}$ N and $\varepsilon = \{0.2, 0.5, 0.8\}$, respectively.

The Nyquist charts of Figures 9 and 10 reveal some interesting features. The most obvious is the occurrence of a jumping phenomenon, which is a characteristic of nonlinear systems. This phenomenon is more visible around $\varepsilon \approx 0.5$, while for the limiting cases, that is $\varepsilon \to 0$ and $\varepsilon \to 1$, the singularity disappears.

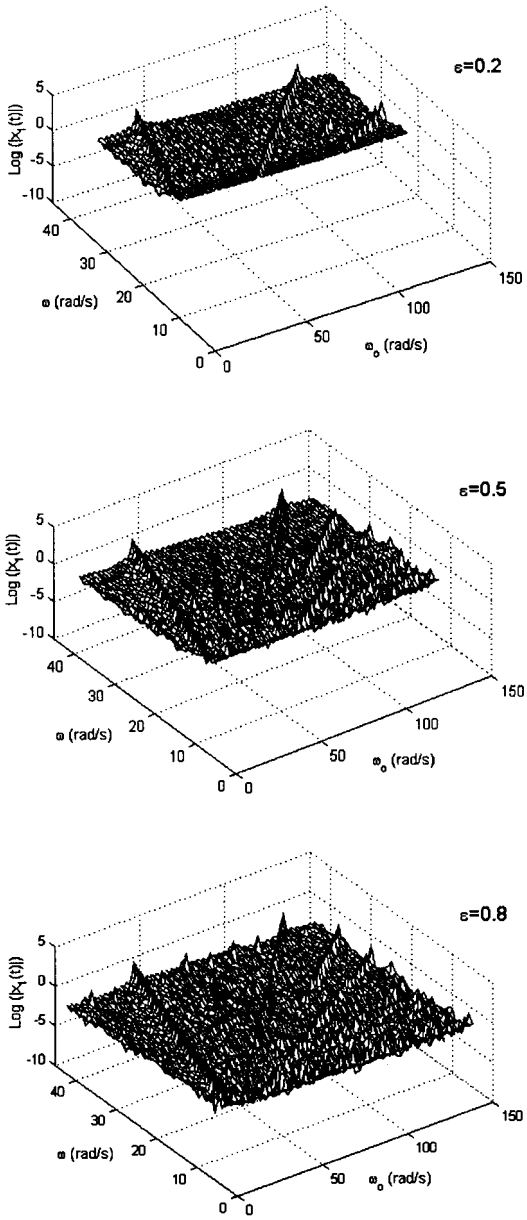

Figure 11. Fourier transform of the output displacement $x_1(t)$, over 500 cycles, vs. the exciting frequency ω and the harmonic frequency ω_0, for $\varepsilon = \{0.2, 0.5, 0.8\}$.

The frequency for which the jumping phenomena occurs (ω_J) has the relation:

$$\omega_J \sim \left(\frac{F}{h \cdot M_2}\right)^{1/2}. \tag{15}$$

Moreover, Figure 10 shows also that for a fixed value of ε the charts are proportional to the input amplitude F.

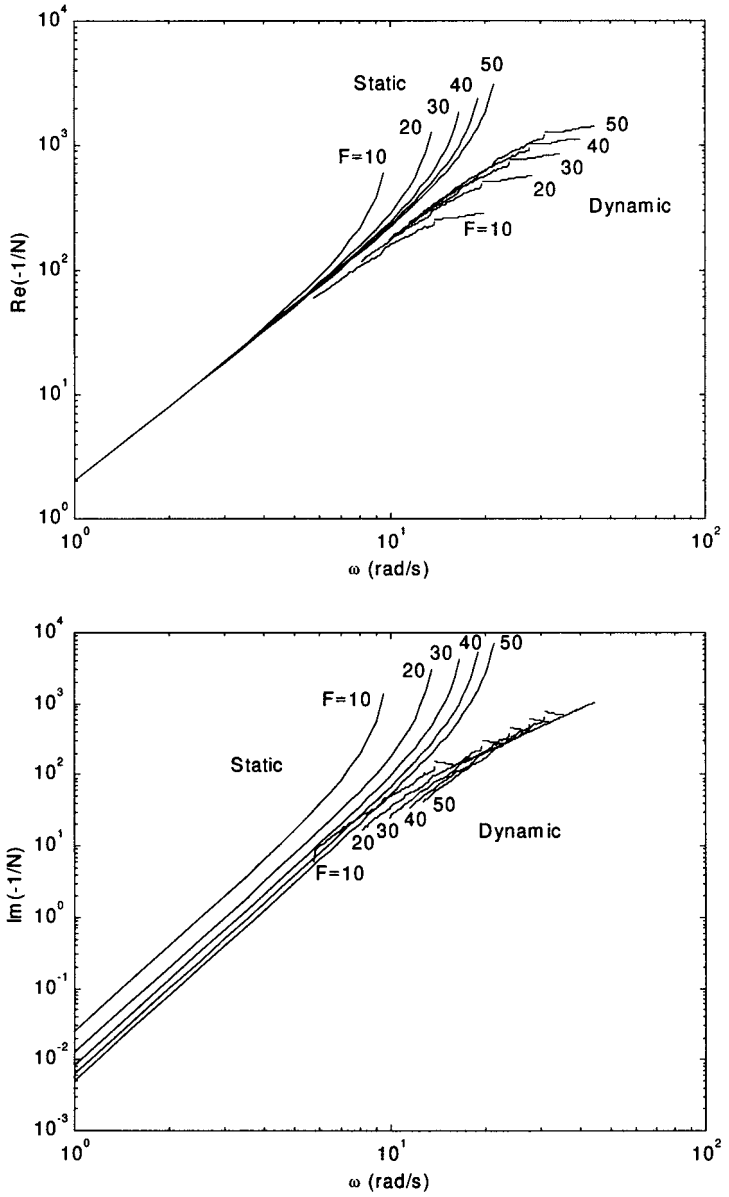

Figure 12. Log-log plots of $\mathrm{Re}\{-1/N\}$ and $\mathrm{Im}\{-1/N\}$ vs. the exciting frequency ω, for $\varepsilon = 0.5$ and $F = \{10, 20, 30, 40, 50\}$ N.

Figure 11 presents the harmonic content of $x_1(t)$ for an input force $f(t) = 50\cos(\omega t)$, $\omega_C < \omega < \omega_L$, and $\varepsilon = \{0.2, 0.5, 0.8\}$. The charts demonstrate that the fundamental harmonic of the output has a much higher magnitude than the other higher-harmonic components. This fact supports the application of the describing function method in the prediction of limit cycles for this system. Note also that for large values of the coefficient of restitution (e.g. $\varepsilon = 0.8$), the high-order harmonic content increases and, by consequence, the accuracy of the prediction diminishes.

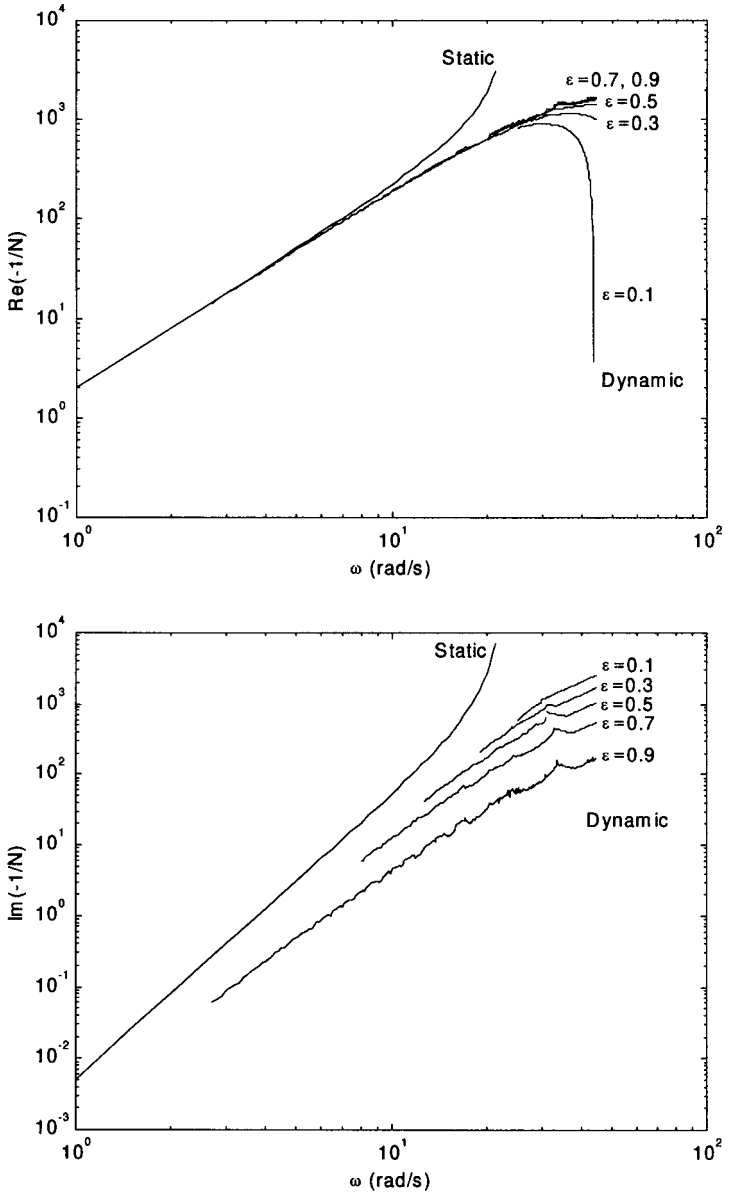

Figure 13. Log-log plots of $\mathrm{Re}\{-1/N\}$ and $\mathrm{Im}\{-1/N\}$ vs. the exciting frequency ω, for $F = 50$ N and $\varepsilon = \{0.1, 0.3, 0.5, 0.7, 0.9\}$.

Figures 12 and 13 illustrate the variation of the Nyquist plots of $-1/N(F, \omega)$ for the cases of the static and dynamic backlash. Figure 12 shows the log-log plots of $\mathrm{Re}\{-1/N\}$ and $\mathrm{Im}\{-1/N\}$ vs. ω for a constant coefficient of restitution $\varepsilon = 0.5$ and $F = \{10, 20, 30, 40, 50\}$ N, while Figure 13 depicts the log-log plots of $\mathrm{Re}\{-1/N\}$ and $\mathrm{Im}\{-1/N\}$ vs. ω for a constant input force $F = 50$ N and $\varepsilon = \{0.1, 0.3, 0.5, 0.7, 0.9\}$.

Comparing the results for the static and the dynamic backlash models we conclude that:

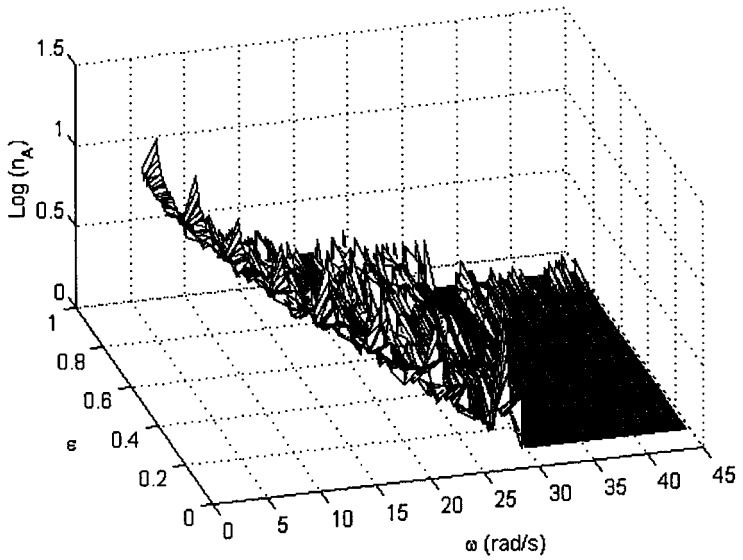

Figure 14. Number of consecutive collisions on side A (n_A) vs. the exciting frequency ω and the coefficient of restitution ε, for an input force $f(t) = 50\cos(\omega t)$. For the side B (n_B) the chart is of the same type.

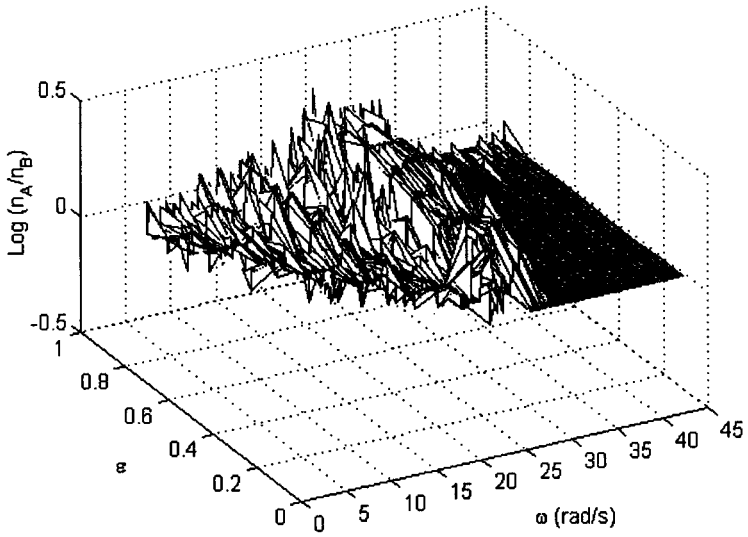

Figure 15. Ratio of the number of consecutive collisions on side A (n_A) and side B (n_B), n_A/n_B, vs. the exciting frequency ω and the coefficient of restitution ε, for an input force $f(t) = 50\cos(\omega t)$.

- The charts of $\mathrm{Re}\{-1/N\}$ are similar for low frequencies (where they reveal a slope of $+40$ dB/dec) but differ significantly for high frequencies.
- The charts of $\mathrm{Im}\{-1/N\}$ are different in all range of frequencies. Moreover, for low frequencies, the dynamic backlash has a fractional slope inferior to $+80$ dB/dec of the static model.

A careful analysis must be taken because it was not demonstrated that a DF fractional slope would imply a fractional-order model. In fact, in this study we adopt integer-order models for

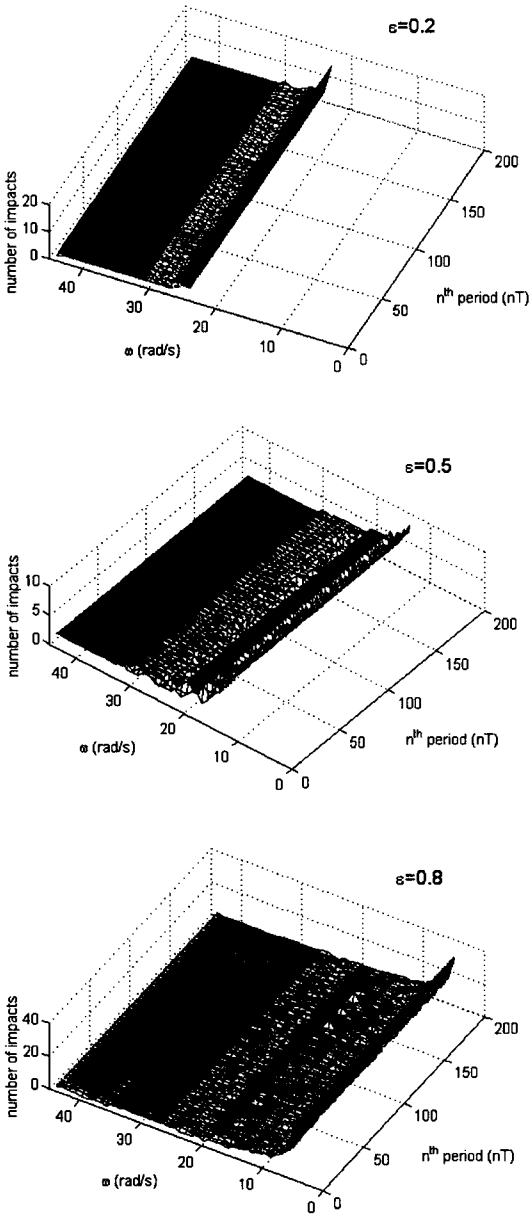

Figure 16. Number of impacts per excitation period $T = 2\pi/\omega$ considering three values of $\varepsilon = \{0.2, 0.5, 0.8\}$ and a constant input force $F = 50$ N.

the system description but the fractional-order slope is due to continuous/discrete dynamic variation that results due to the mass collisions. Consequently, a complementary perspective for the characterization of the system behavior is given through the analysis of the number of impacts that occur.

Figure 14 depicts n_A (or n_B), the number of consecutive collisions on side A (or B), vs. the exciting frequency ω and the coefficient of restitution ε. A plot of the same type is given

in Figure 15 and relates the ratio of the number of consecutive collisions on sides A and B, n_A/n_B, vs. (ω, ε) for an input force $f(t) = 50\cos(\omega t)$.

The results show that:

- For $\omega_C < \omega < \omega_J$ the system is characterized by an irregular number of impacts and a chaotic dynamics.
- For $\omega_J < \omega < \omega_L$ the motion is characterized by a regular behaviour corresponding to one alternate collision on each side of M_1.

We observe that a large part of the graph is characterized by a relation $1 < n_A < 2$ (or $2 > n_B > 1$) and that the jumping phenomenon (that occurs for $\omega = \omega_J$) corresponds to a change on the relation from $n_A/n_B = 1/2$ up to $n_A/n_B = 1$.

We can also analyze the number of collisions per period $T = 2\pi/\omega$ of the exciting frequency ω. Figure 16 depicts the number of impacts for different values of the coefficient of restitution $\varepsilon = \{0.2, 0.5, 0.8\}$. Once again, we note that the graphs show two kinds of regions. The 'rough regions' are characterized by an irregular number of impacts that correspond to the chaotic dynamics. The 'soft regions' are characterized by a regular number of impacts and a periodic motion of the system. Note also that the higher the coefficient of restitution ε (e.g. $\varepsilon = 0.8$) the more scattered are the chaotic regions.

4. Conclusions

This paper addressed several aspects of the phenomena involved in systems with backlash and impacts. The dynamics of a two-mass system was analyzed through the describing function and compared with standard models. The results revealed that these systems might lead to chaos and to fractional-order dynamics. These conclusions encourage further studies of nonlinear systems in the perspective of the fractional calculus since integer-order dynamical models are not capable to take into account many phenomena that occur.

References

1. Oldham, K. B. and Spanier, J., *The Fractional Calculus: Theory and Application of Differentiation and Integration to Arbitrary Order*, Academic Press, New York, 1974.
2. Samko, S. G., Kilbas, A. A., and Marichev, O. I., *Fractional Integrals and Derivatives: Theory and Applications*, Gordon and Breach, Amsterdam, 1993.
3. Miller, K. S. and Ross, B., *An Introduction to the Fractional Calculus and Fractional Differential Equations*, Wiley, New York, 1993.
4. Podlubny, I., *Fractional Differential Equations*, Academic Press, San Diego, CA, 1999.
5. Hilfer, R., *Applications of Fractional Calculus in Physics*, World Scientific, Singapore, 2000.
6. Ross, B. , *Fractional Calculus and Its Applications*, Lecture Notes in Mathematics, Vol. 457, Springer-Verlag, New York, 1974.
7. Samko, S. G. and Ross, B., 'Integration and differentiation to a variable fractional order', *Integral Transforms and Special Functions* **1**(4), 1993, 277–300.
8. Gemant, A., 'A method of analyzing experimental results obtained from elasto-viscous bodies', *Physics* **7**, 1936, 311–317.
9. Stiassnie, M., 'On the application of fractional calculus for the formulation of viscoelastic models', *Applied Mathematical Modelling* **3**, 1979, 300–302.

10. Bagley, R. L. and Torvik, P. J., 'Fractional calculus – A different approach to the analysis of viscoelastically damped structures', *AIAA Journal* **21**(5), 1983, 741–748.
11. Bagley, R. L. and Torvik, P. J., 'On the fractional calculus model of viscoelastic behaviour', *Journal of Rheology* **30**(1), 1986, 133–155.
12. Bagley, R. L. and Calico, R. A., 'Fractional order state equations for the control of viscoelastically damped structures', *ASME Journal of Guidance* **14**(2), 1991, 304–311.
13. Fenander, Å., 'Modal synthesis when modeling damping by use of fractional derivatives', *AIAA Journal* **34**(5), 1996, 1051–1058.
14. Hartley, T. T., Lorenzo, C. F., and Qammer, H. K., 'Chaos in fractional order Chua's system', *IEEE Transactions on Circuits and Systems – I: Fundamental Theory and Applications* **42**(8), 1995, 485–490.
15. Liu, S. H., 'Fractal model for the ac response of a rough interface', *Physical Review Letters* **55**(5), 1985, 529–532.
16. Kaplan, T., Gray, L. J., and Liu, S. H., 'Self-affine fractal model for a metal-electrolyte interface', *Physical Review B* **35**(10), 1987, 5379–5381.
17. Méhauté, A., *Fractal Geometries: Theory and Applications*, Penton Press, London, 1991.
18. Anastasio, T. J., 'The fractional-order dynamics of brainstem vestibulo-oculomotor neurons', *Biological Cybernetics* **72**, 1994, 69–79.
19. Oustaloup, A., 'Fractional order sinusoidal oscillators: Optimization and their use in highly linear FM modulation', *IEEE Transactions on Circuits and Systems* **28**(10), 1981, 1007–1009.
20. Ozaktas, H. M., Arikan, O., Kutay, M. A., and Bozdagi, G., 'Digital computation of the fractional Fourier transform', *IEEE Transactions on Signal Processing* **44**(9), 1996, 2141–2150.
21. Nigmatullin, R. R., 'The realization of the generalized transfer equation in a medium with fractal geometry', *Physics of the State Solid (b)* **133**, 1986, 425–430.
22. Méhauté, A., Héliodore, F., Cottevieille, D., and Latreille, F., 'Introduction to wave phenomena and uncertainty in a fractal space', *Chaos, Solitons & Fractals* **3**(5), 1993, 389–402.
23. Mainardi, F., 'Fractional relaxation-oscillation and fractional diffusion-wave phenomena', *Chaos, Solitons & Fractals* **7**(9), 1996, 1461–1477.
24. Méhauté, A., 'From dissipative and to non-dissipative processes in fractal geometry: The janals', *New Journal of Chemistry* **14**(3), 1990, 207–215.
25. Matignon, D. and d'Anréa-Novel, B., 'Some results on controllability and observability of finite-dimensional fractional differential systems', in *Proceedings IEEE SMC/IMACS Symposium on Control, Optimization and Supervision*, Lille, France, P. Borne, M. Staroswiecki, J. F. Cassae, and S. L. Khattiabi (eds.), IEEE, New York, 1996, pp. 952–956.
26. Mathieu, B., Le Lay, L., and Oustaloup, A., 'Identification of non integer order systems in the time domain', in *Proceedings IEEE SMC/IMACS Symposium on Control, Optimization and Supervision*, Lille, France, P. Borne, M. Staroswiecki, J. F. Cassae, and S. L. Khattiabi (eds.), IEEE, New York, 1996, pp. 843–847.
27. Engheta, N., 'On the role of fractional calculus in electromagnetic theory', *IEEE Antennas and Propagation Magazine* **39**(4), 1997, 35–46.
28. Engheta, N., 'Fractional paradigm in electromagnetic theory', in *Frontiers of Electromagnetics*, D. H. Werner and R. Mittra (eds.), IEEE, New York, 1999, pp. 523–552.
29. Oustaloup, A., *La Dérivation Non Entière*, Hermes, Paris, 1995.
30. Machado, J. A. T., 'Analysis and design of fractional-order digital control systems', *SAMS Journal Systems Analysis, Modelling, Simulation* **27**, 1997, 107–122.
31. Machado, J. A. T., 'Discrete-time fractional-order controllers', *FCAA Fractional Calculus and Applied Analysis* **4**(1), 2001, 47–66.
32. Vinagre, B. M., Podlubny, I., Hernández, A., and Feliu, V., 'Some approximations of fractional order operators used in control theory and applications', *FCAA Fractional Calculus and Applied Analysis* **3**(3), 2000, 231–248.
33. Podlubny, I., 'Fractional-order systems and $PI^{\lambda}D^{\mu}$-controllers', *IEEE Transactions on Automatic Control* **44**(1), 1999, 208–213.
34. Phillips, C. L. and Harbor, R. D., *Feedback Control Systems*, Prentice-Hall, Englewood Cliffs, NJ, 1991.
35. Slotine, J. E. and Li, W., *Applied Nonlinear Control*, Prentice-Hall, Englewood Cliffs, NJ, 1991.
36. Choi, Y. S. and Noah, S. T., 'Periodic response of a link coupling with clearance', *ASME Journal of Dynamic Systems, Measurement and Control* **111**(2), 1989, 253–259.

37. Stepanenko, Y. and Sankar, T. S., 'Vibro-impact analysis of control systems with mechanical clearance and its application to robotic actuators', *ASME Journal of Dynamic Systems, Measurement and Control* **108**(1), 1986, 9–16.
38. Azenha, A. and Machado, J. A. T., 'On the describing function method and the prediction of limit cycles in nonlinear dynamical systems', *Journal of Systems Analysis, Modelling and Simulation* **33**, 1998, 307–320.